Ultrawide 3D Phononic Bandgap Metastructures as Broadband Low Frequency Filter

Muhammad
City University of Hong Kong
C.W. Lim (bccwlim@cityu.edu.hk)
City University of Hong Kong

Research Article

Keywords: 3D bandgap, additive manufacturing, phononic metastructure

Posted Date: December 1st, 2020

DOI: https://doi.org/10.21203/rs.3.rs-114173/v1

Version of Record: A version of this preprint was published at Scientific Reports on March 30th, 2021. See the published version at https://doi.org/10.1038/s41598-021-86520-8.

Ultrawide 3D Phononic Bandgap Metastructures as Broadband Low Frequency Filter

Muhammad[1,2] and C.W. Lim[1,2,*]

[1]City University of Hong Kong Shenzhen Research Institute, Shenzhen, P.R. China

[2]Department of Architecture and Civil Engineering, City University of Hong Kong, Kowloon, Hong Kong SAR, P.R. China

*Corresponding author email: bccwlim@cityu.edu.hk

Graphical Abstract

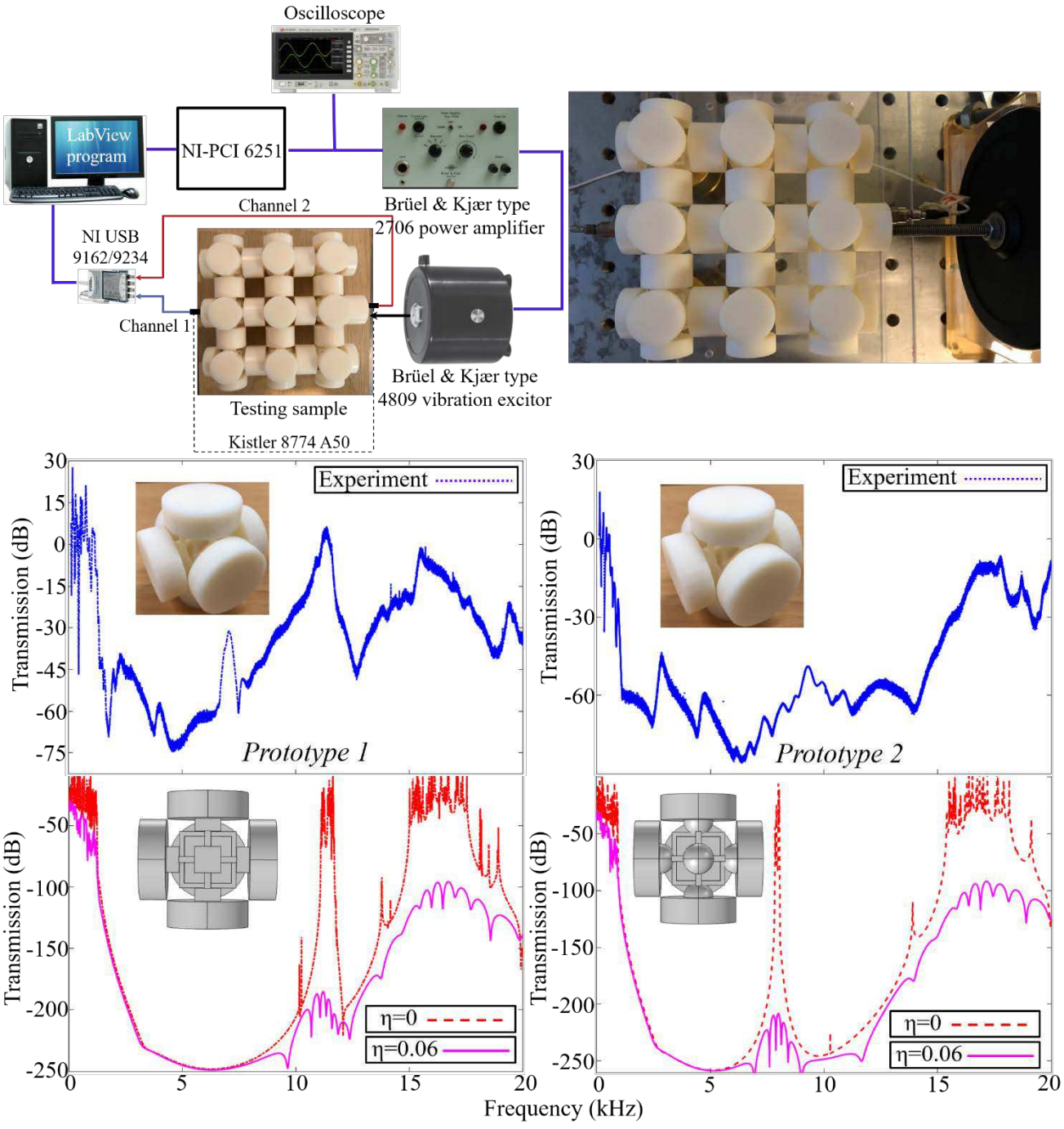

Ultrawide 3D Phononic Bandgap Metastructures as Broadband Low Frequency Filter

Muhammad[1,2] and C.W. Lim[1,2,*]

[1]City University of Hong Kong Shenzhen Research Institute, Shenzhen, P.R. China

[2]Department of Architecture and Civil Engineering, City University of Hong Kong, Kowloon, Hong Kong SAR, P.R. China

*Corresponding author email: bccwlim@cityu.edu.hk

Highlights

- A novel metastructure prototype governing extremely wide three-dimensional bandgaps is established.
- By principal of mode separation, the phenomenon of bandgap generation is explained.
- The opening of bandgap is studied through analytical formulation and finite element simulations.
- By additive manufacturing 3D printed prototypes are prepared and wave attenuation over ultrawide frequency region is validated.
- The analytical model, numerical codes and vibration test on 3D printed prototypes showed excellent agreement.

Ultrawide 3D Phononic Bandgap Metastructures as Broadband Low Frequency Filter

Muhammad[1,2] and C.W. Lim[1,2,*]

[1]City University of Hong Kong Shenzhen Research Institute, Shenzhen, P.R. China

[2]Department of Architecture and Civil Engineering, City University of Hong Kong, Kowloon, Hong Kong SAR, P.R. China

*Corresponding author email: bccwlim@cityu.edu.hk

Abstract

This present study reports a novel model for the study on three-dimensional phononic metastructures endued with ultrawide three-dimensional complete bandgaps. The phononic structure is made of a unique material without composite material composition. Based on the principal of mode separation and global and local modal masses participation, the well-engineered structural configurations give extremely wide bandgaps with the gap-to-mid gap ratio of 157.6% and 160.1% for two proposed prototypes that produce the widest three-dimensional bandgaps ever reported. The band structures are explained by a modal analysis and the findings are further corroborated by developing an analytical model based on monoatomic mass-spring chain and further verified with well-established FEM numerical simulations. Thanks to additive manufacturing, the prototypes are developed by using 3D printing technology and low amplitude vibration test is performed to access the real-time vibration mitigation characteristics. An excellent agreement is obtained between analytical, numerical and experimental results. The effects of material damping on transmission response is also taken into consideration that eventually merge the separated bandgaps to form a broadband vibration attenuation zone. The results reported are scale independent and the proposed strategy may pave the way for developing novel meta-devices to control the noise and vibration, and underwater acoustic waves at a wide frequency band in all directions.

Keywords: 3D bandgap; additive manufacturing; phononic metastructure

Artificial periodic structures that once begin from electromagnetic media are presently hot research topics for noise and vibration control due to their unprecedented dynamic mechanical properties that are inconceivable with respect to natural materials[1,2]. The key property of interest includes formation of bandgap (BG) that is a frequency region where incident wave propagation is prohibited. Although waveguiding[3], focusing and collimation[4], negative refraction[5],topological properties[6-8] and underwater acoustic applications [9-11] have been explored, the multi-directional vibration control with extremely wide complete BG is also intriguing. Multiple approaches including single material[12,13] and elastic impedance based multi-materials periodic structures by active[14] and passive[15-17] control techniques have been proposed to enlarge the BGs. Among those approaches the recently emerging 3D phononic structures with complete 3D BG[18-20], inertial amplification phenomena[12], actively controlled piezo-patches technique[14,21,22], elastic metamaterials with dissipative medium characteristics[16] and multi-resonant trampoline metamaterials[15] with trampoline effect[23] have caught extensive attentions. The relative bandwidth $\Delta\omega/\omega_c$ or gap to mid-gap ratio is among the quantitative measures to determine the performance and robustness of BGs, i.e. a wider BG attenuates wave energy over a wide range of frequency. The width of BG is expressed by $\Delta\omega/\omega_c = 2\left(\omega_t - \omega_b\right)/\omega_t + \omega_b$ [24,25] where ω_t and ω_b are the top and bottom bounding edge frequencies, respectively. Table 1 shows a brief summary for the widest BG reported to date.

Table 1: The widest BGs reported

Reference	Composition type	Working direction	$\Delta\omega/\omega_c$
Barnhart[16]	Multi-material	1D	58%
Zhou[14]	Multi-material	1D	155%
Muhammad[15]	Multi-material	2D	92%-29%
Acar[12]	Single-material	2D	74%
Muhammad[24]	Multi material	2D	150%
Lu[26]	Multi-material	3D	100%
D'Alessandro[18]	Single material	3D	132%
D'Alessandro[27]	Single material	3D	134.7%
D'Alessandro[20]	Single material	3D	63.8%-74.1%

Although locally resonant multi-core structures induce wider BGs in those reported works, the width of BG largely depends upon the mass of resonator/scatterer and impedance mismatch. For a wider BG, a larger-sized resonator is required. Further, in the works as shown in Table

1, more focus is devoted for obtaining a wide BG from 1D and 2D periodic lattices/structures[14,28,29]. Recently, 3D periodic structures consisting of multi-core materials are also proposed to maximize the impedance mismatch in order to achieve wider BGs[17,30]. In such approach, multi-material based prototyping and/or adjusting the assembly phase of materials pose a significant challenge. For a single core structure, this milestone constitutes a significant advancement in terms of structure optimization to adjust the filling ratio between material regions and voids. In this regard, the present work proposes two phononic metastructure prototypes that consist of a single core structure and it is capable of inducing extremely wide BG in all three directions of the irreducible Brillouin zone. We adopt the principal of mode separation[31] where the structural components consist of rigid masses and elastic beams/frames resembling the conventional monoatomic mass-spring system to design the periodic structures [1]. We demonstrated the vibration mitigation capability from those structures both numerically and experimentally. For the details of theoretical framework, governing equations and design optimization, one can refer to the *supplementary materials.* In this study, first, an analytical model is developed to calculate the acoustic mode frequency responsible for opening the BG[1] and then a finite element based numerical technique is implemented to obtain the band structures and frequency response spectra. By additive manufacturing technology, the 3D prototypes are printed and vibration tests are performed to validate the presence and effectiveness of ultrawide three-dimensional BGs.

Prototypes and modal comparison

The topology in Fig. 1(a) shows 3D optimized phononic metastructures that are designed in a single material in terms of $\Delta\omega/\omega_c$ for in-plane elastic wave propagation. In both prototypes, the unit cell topology is realized by an external frame assembly connected with cylindrical masses at the middle points. The optimized structures have the following internal properties: frame assembly thickness $w_b = 0.035a$, $w_h = 0.045a$ that is connected with a cylindrical mass of radius $r = 0.3a$ and height $h = 0.65r$ via a small cube of side length $l_c = 0.19a$ for *Prototype 1* or an equivalent volume sphere with diameter d for *Prototype 2*. One half of the cube/sphere is embedded inside the cylindrical mass and the other half is connected to the frame assembly. The cube/sphere is introduced for two reasons: (i) it provides strong support between the frame assembly and cylindrical masses; and (ii) it optimizes $\Delta\omega/\omega_c$ that gives a wider BG. Further, all geometric parameters are presented in terms of the lattice constant $a = 0.05\text{m}$. For numerical modelling and additive manufacturing, VeroWhite (Young

modulus $E = 1.6\,\text{GPa}$, mass density $\rho = 1174\ \text{kg/m}^3$ and Poisson's ratio $\nu = 0.33$ Stratasys Ltd) is used. For simplicity, the band structures are presented in the form of a general frequency f and a normalized frequency $f_{nd} = fa/v$ where $v = \sqrt{E/\rho}$ is the longitudinal wave velocity. Subsequently dynamic mechanical test is performed to determine the material loss factor η that is required for the investigation of effect of material damping on numerically obtained transmission curves, see *supplementary information*. We obtained the frequency response spectra by FE approach using COMSOL Multiphysics 5.4® and ANSYS 2020 R1®. For *Prototype 1* the analytical model and FE results are compared in Table. 2. One can observe an excellent agreement between the two models.

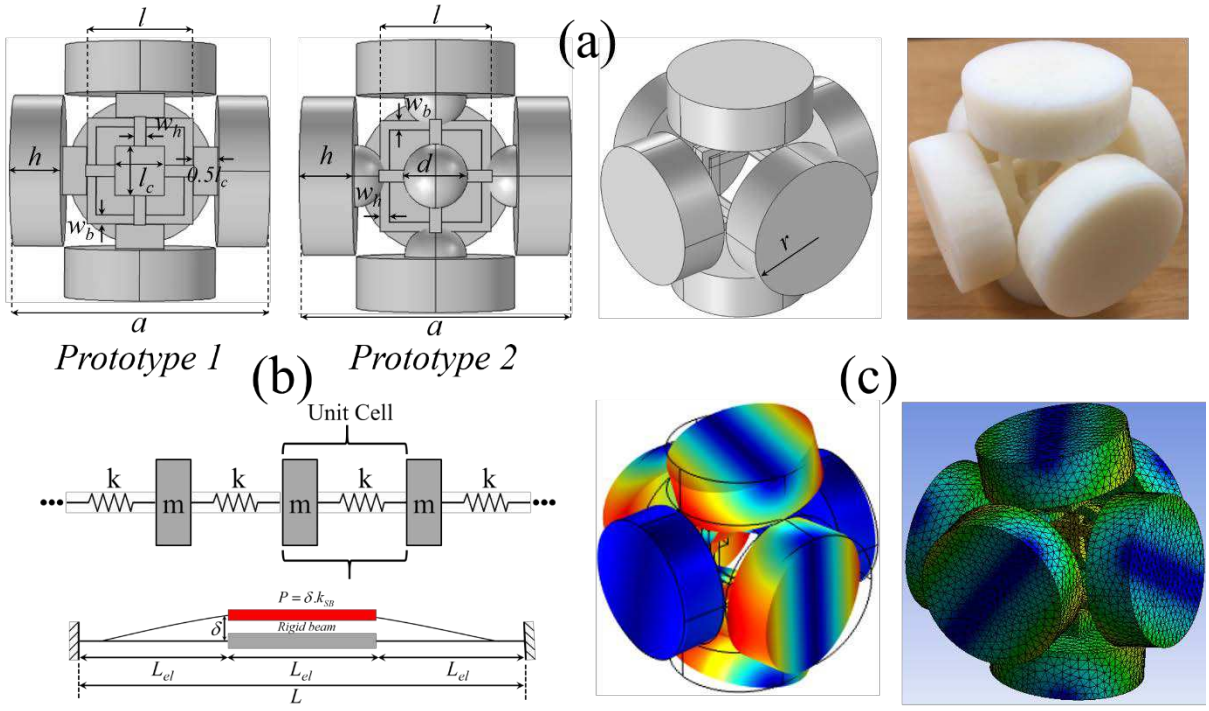

Fig. 1. Proposed prototypes for 3D phononic metastructures. (a) Schematic description for prototype 1-2 with 3D printed sample. (b) Monoatomic mass-spring chain along with simplified beam structure. (c) Vibration mode for the lower bounding edge of first BG by COMSOL Multiphysics 5.4® (left) and ANSYS 2020 R1® (right). The analytical and FEA results comparison is presented in Table. 2.

Table 2: Comparison of different FE models

	Analytical Model	COMSOL Multiphysics®	ANSYS 2020 R1®
Prototype 1	1279.2 Hz (0.05478)	1247.2 Hz (0.05341)	1240 Hz (0.05312)

The modal analysis by both FE codes shows a dominant mixed compressional-bending resonant mode that initiates BG where the cylindrical masses and cubes/spheres work as rigid masses while box-like frame assembly exploits the flexural stiffness of frame assembly when subjected to incident elastic waves. For better understanding, a monoatomic mass-spring chain is introduced as shown in Fig. 1(b). For details, see *supplementary information.* For a general monoatomic mass-spring chain, the acoustic mode frequency ω responsible for opening the BG is $\omega = 2\omega_0$ and $\omega_0 = \sqrt{k/m}$ is natural frequency of the system[1]. For present monoatomic chain the acoustic mode frequency is $f_{nd} = 2/2\pi\sqrt{k/m}\left(a/v\right)$ that is listed in Table. 2. The parameter m incorporates the mass of cylinders and cube for *Prototype 1* or sphere for *Prototype 2* while k represents the longitudinal stiffness of supporting frame structure with $k = \kappa\gamma k_{SB}$. Here κ and γ are associated with the stiffness of two sets of beams and the summation of two orthogonal beam stiffnesses, respectively, that are connected with cylindrical masses via cubes/spheres. For the present symmetric frame assembly $\kappa = 0.5$ and $\gamma = 2$[31]. Furthermore, as shown in Fig. 1(b), for a single beam with the effective length $L_{el} = L/3 - w_b/2$ the stiffness is $k_{SB} = 24EI/L_{el}^3$ where $I = \frac{1}{12}w_b w_h^3$ is second moment of area and L_{el} is beam effective length. The results comparison for *Prototype 1* is presented in Table 2 and there exists an error of 2.5-3% between numerical and analytical solutions for the opening edge of the first BG. For *Prototype 2* the BG opening edge obtained from COMSOL Multiphysics® and ANSYS 2020 R1® are 929.24 Hz (0.03981) and 939.86 Hz (0.04026), respectively. The vibration modes obtained from COMSOL and ANSYS is shown in Fig. 1(c) to double check the accuracy. An excellent agreement can be observed in term of deformation mechanism and displacement field distribution. Further details can be found in the *supplementary materials*.

Results and discussion

For *Prototype 1*, the numerical band structure and BGs determined by COMSOL Multiphysics5.4® is shown in Fig. 2(a-b). The first BG is the widest with the relative bandwidth 160.2%. The vibration modes corresponding to the bounding BG edges are shown in Fig. 2(c). The vibration modes associated to BG opening and closing edges are designated with red and green stars, respectively. The single material 3D structure proposed here possesses the widest 3D BG with the capability of attenuating mechanical vibration and noise in all directions as compared to the reported works listed in Table. 1.

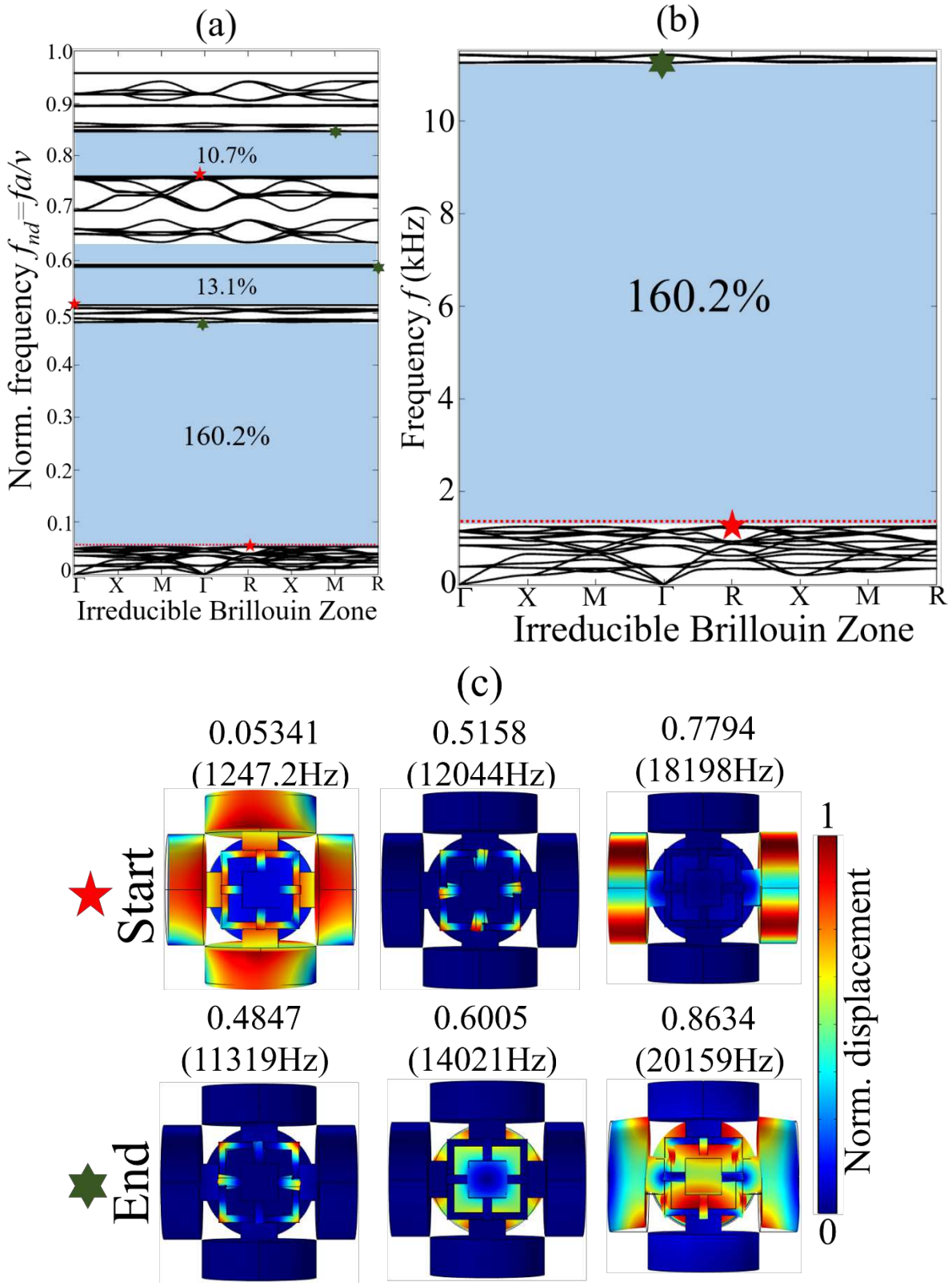

Fig. 2. *Prototype 1*- numerical dispersion spectra: (a) complete band structure with normalized frequency; (b) the widest first BG with $\Delta\omega/\omega_c$ of 160.2%; (c) vibration modes corresponding to the lower and upper bounding edges of BGs.

Similarly, the band structure with BGs and vibration modes corresponding to the bounding BG edges for *Prototype 2* are shown in Fig. 3 (a-c). It is noticed that replacing cube masses with spheres of an equivalent volume results in two wide BGs with $\Delta\omega/\omega_c$ 157.6% and 55%, respectively. Interestingly both BGs are very close and they are separated by some narrow passbands. The material damping/viscoelasticity effects will weaken this passband that eventually results in a broadband BG covering an extremely wide frequency range.

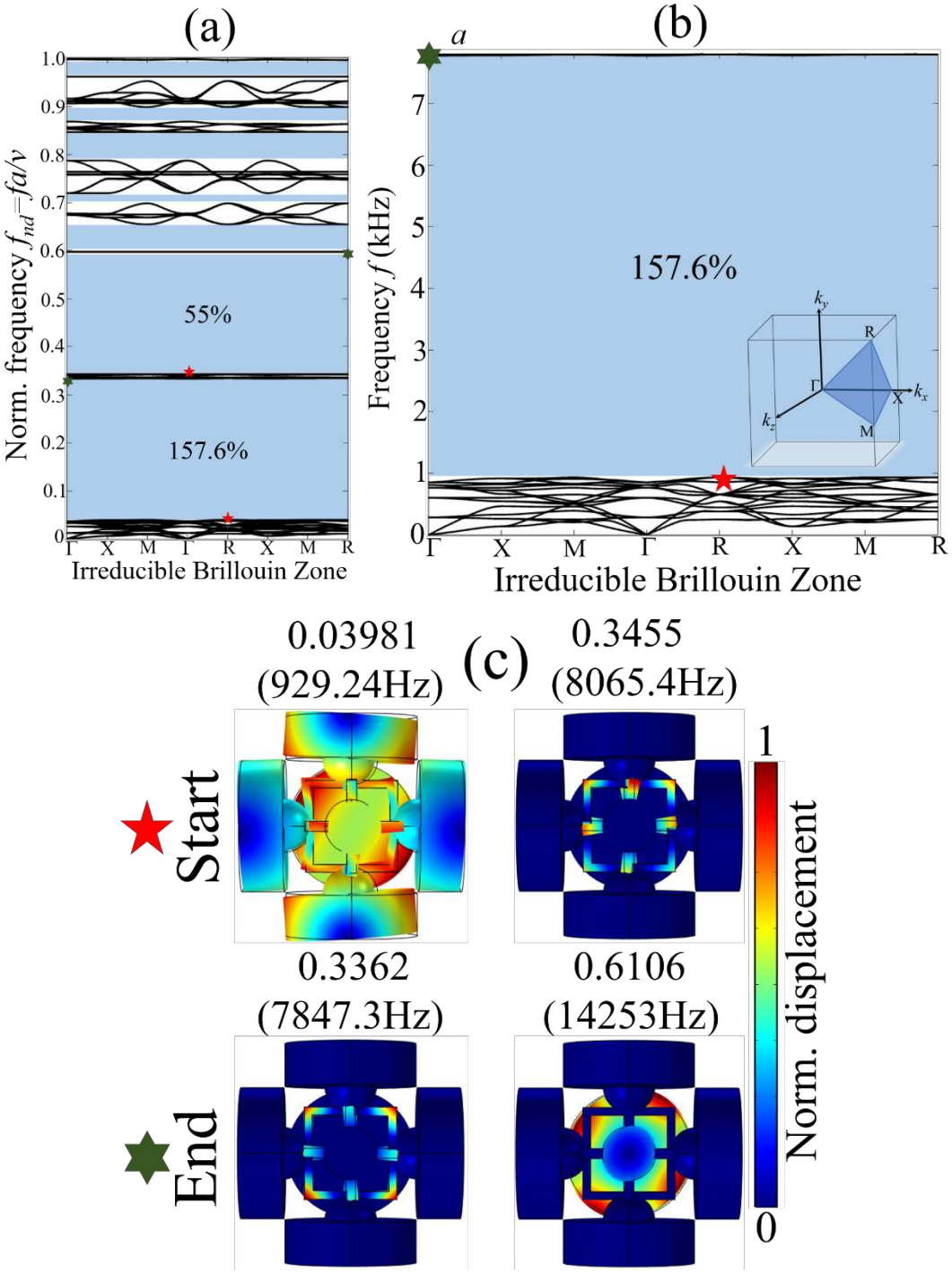

Fig. 3. *Prototype 2*- numerical dispersion spectra: (a) complete band structure with normalized frequency; (b) the widest first BG with $\Delta\omega/\omega_c$ of 157.6%; and (c) vibration modes corresponding to the lower and upper bounding edges of BGs.

For both *Prototype 1* and *Prototype 2*, the nature of the widest first BG is due to structural optimization. Significant contribution is made by the rigid masses and flexural stiffness of the frame assembly as indicated by the vibration modes. Further, the mechanical features of these modes (i.e deformation mechanism of modal stiffness and modal masses) are identical at different points within a particular band in the irreducible Brillouin zone. However, with a change in the wave propagation direction, the deformation phase varies but the deformation mechanism remains identical. In addition, for both prototypes the modal analysis result also indicates that significant contribution is made by the complete unit cell for the lower bounding edge of the first BG. In other words, the rigid motion of lumped cylindrical-cube/sphere masses and flexural deformation of elastic frame assembly play an important role in the opening of the first BG. Since the complete unit cell structures are in vibration, thus we call it a global resonant mode. Also, due to involvement of complete unit cell structure, the effective mass increases and eigenmode is situated at relatively lower frequency region. The analytical model also validates this finding as shown in Fig. 1(b).

In contrast, for the closing bounding edge of the first widest BG as shown in Fig. 2(c) and Fig. 3(c), the rigid masses remain almost unaffected while the vibration mode is characterized by local deformation of the frame-like beam assembly. Here, we call it a local resonant mode where vibration is observed only in frame assembly. A comparison between these two opening and closing BG edges indicate the modal mass participation in the closing BG edge is much smaller than the opening counterpart mode while the flexural stiffness of the frame assembly has reminiscent effect. Thus, due to insufficient modal mass participation and flexural deformation of elastic frame assembly, the upper bounding BG edge is located at a significantly higher frequency compare to the BG opening mode. In summary, the structural optimization results in significant difference between the opening (global resonant mode) and closing (local resonant mode) of BG edges that gives ultrawide BG. In the present study, we intend to optimize the difference between global and local resonant modes to obtain an extremely wide BG. Thus, modal masses participation and flexural stiffness of supporting frame assembly in the proposed 3-D prototypes play an important role for the opening and closing of BG. A similar conclusion can be derived from the vibration modes for higher BGs where the

contribution of rigid masses and flexural stiffness of frame-assembly can be seen. Except the lower bounding edge of the first BG, all other BGs have an almost negligible effect from the modal masses hence they are positioned in a higher frequency region. For preliminary designs and optimizations, one can refer to the *supplementary materials.*

Frequency response spectrum

The band structure presented above is obtained from COMSOL Multiphysics® where the Floquet-Bloch periodicity condition is applied on all edges of cylindrical mass that made the structure infinitely periodic in the *x*-*y*-*z* directions. Some reported studies[14,15,20,27,29] indicate one possible way to visualize the vibration mitigation capability from the proposed metastructures is to build a finite array of unit cells and to perform a frequency response study. In this regard, a 3x3x1 supercell structure is constructed. As shown in Fig. 4(a), a harmonic excitation force is applied at the left-edge and the response in the form of displacement is record at the right-edge. The input and output displacement fields are recorded with the help of probes and the transmission ratio $T = 20\log_{10}\left(u_{\text{out}}/u_{\text{in}}\right)$ is calculated.

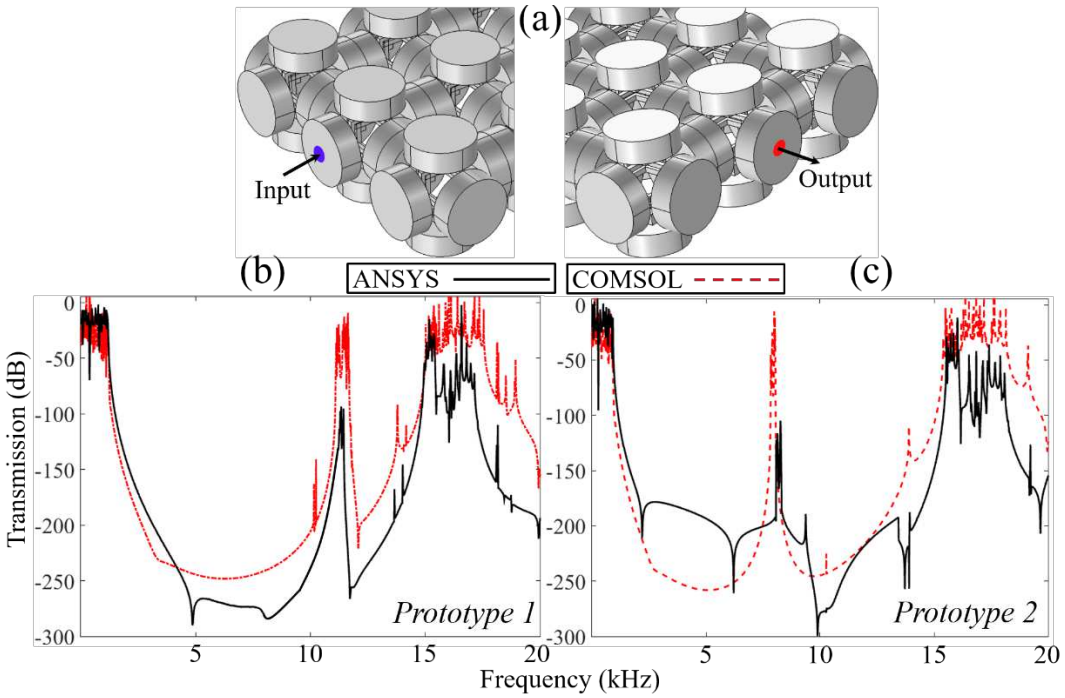

Fig. 4. (a) Finite supercell with input (blue) and output (red) probes; (b-c) response spectrum for *Prototype 1* and *Prototype 2* obtained from COMSOL Multiphysics (red dashed line) and ANSYS workbench (black solid line).

The transmission obtained by FE numerical simulation presented in Fig. 4(b, c) correspond to the $\Gamma - X$ direction of the irreducible Brillouin zone. Since BGs are uniformly distributed in all directions of the Brillouin zone, thus wave propagation in any direction leads to an identical response spectrum. Inside BG, one can physically visualize the vibration attenuation capability from the proposed prototypes. Further, as shown in Fig. 5, different probe positions on *Prototype* 2 are selected to investigate the influence of BG width and attenuation depth. The BG width remains persistent for all the cases while the attenuation depth varies. For probe 1 the attenuation is around -50dB while probe 2-3 being equidistance have identical attenuation depth of around -150dB. Similarly, probe 4-5 have attenuation depth of approximately -250dB. In conclusion, an increase in the number of unit cell robustly attenuate the propagating incident waves.

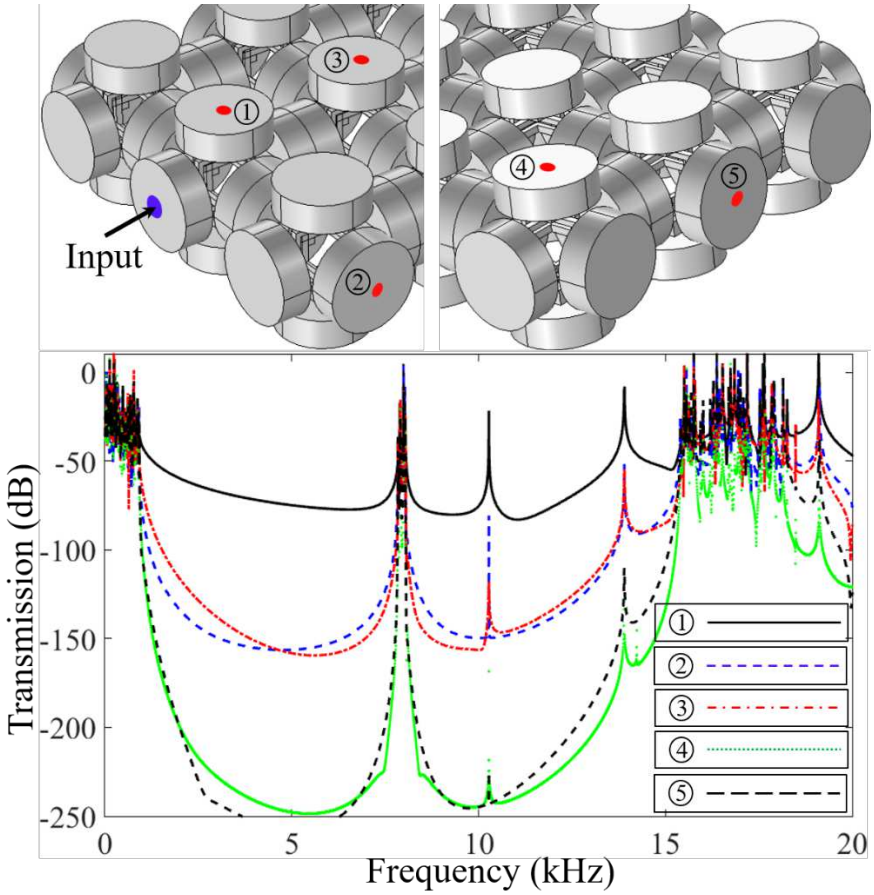

Fig. 5. *Prototype 2:* displacement fields recorded at various probe locations numbered from 1 to 5. The BG width is independent of probe location while the attenuation depth increases if the point probe is away from the excitation source.

The numerical transmission response is first compared by FEA simulations without considering material damping on the response spectrum. The dynamic mechanical analysis

(DMA) test is performed on VeroWhite specimen to determine the material loss factor η [15] and this parameter is incorporated in the FEA codes to investigate the effect of material losses on the BGs. Further details about DMA testing is given in the *supplementary materials*. Thanks to additive manufacturing, by using 3D printer (*Strata sys Ltd*) both prototypes are constructed and a low amplitude vibration test is conducted to investigate the real time vibration attenuation characteristics. In Fig. 6(a), the experiment setup and details are presented[25] while Fig. 6(b-c) compare the numerical and experiment transmission spectra for both prototypes. An excellent agreement between the results is obtained. One can observe identical attenuation bandwidths however due to accelerometers limited precision compare to both FEA codes, there is a discrepancy between numerical and experiment attenuation depth. Other possible reasons for minor discrepancy between numerical and experimental results are (1) manufacturing issues [32,33] and anisotropic feature of the samples (2) back-reflection of the incident waves from the sample boundaries that may have obscure the results. Further, it is observed the presence of η on numerical transmission curve merges the first widest BG with other higher frequency BGs that results in a broadband vibration attenuation zone. This zone is, in fact, much wider than the multi-resonant structures reported previously[15,16].

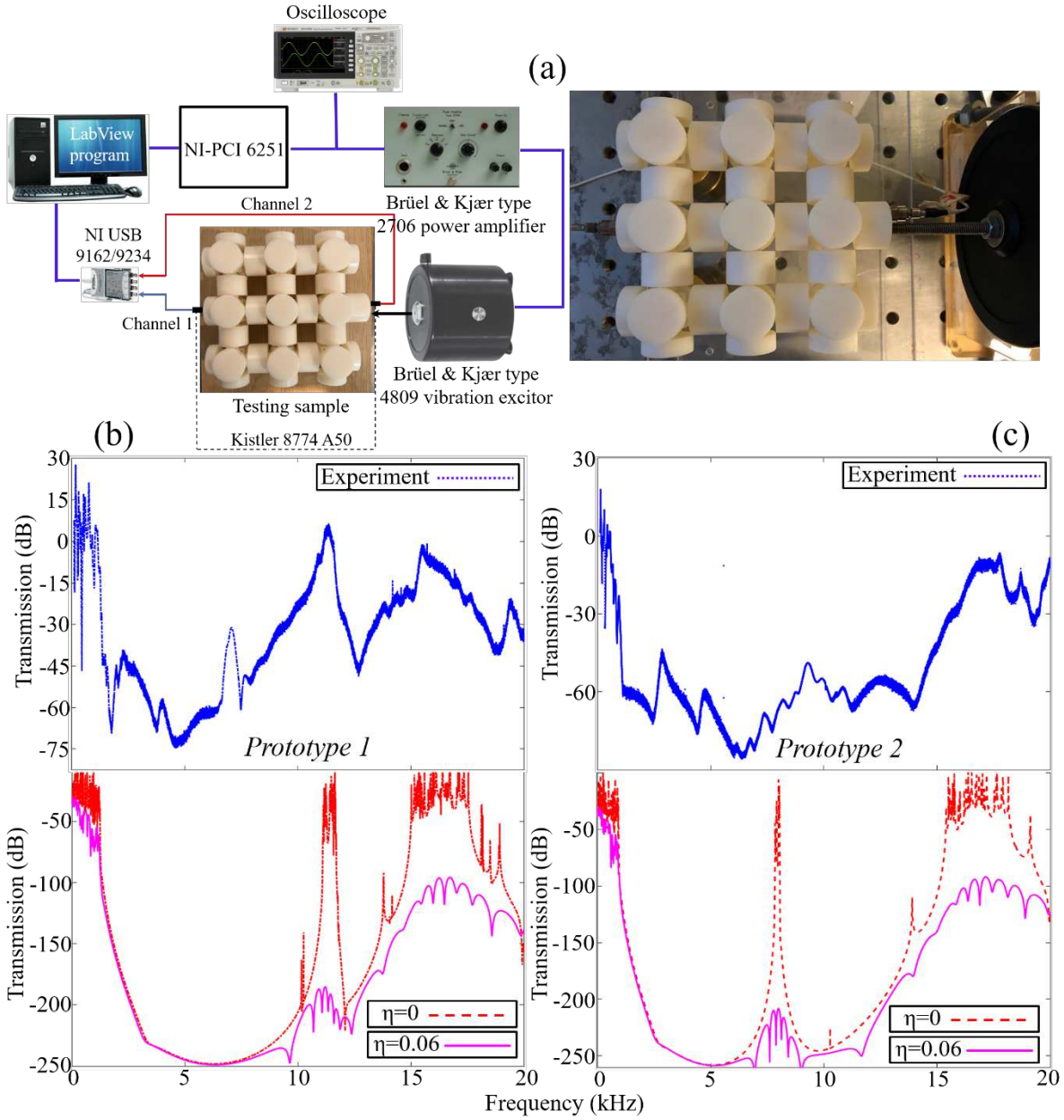

Fig. 6. (a) Experiment setup; (b- c) *Prototype 1* and *Prototype 2* experiment and numerical result. For numerical transmission curve, the effect of material loss factor is $\eta = 0.06$. Excellent agreement between numerical and experiment result is obtained.

Experiment setup

The experiment setup is illustrated in Fig. 6(a) [25]. A vibration excitor (Brüel & Kjær type 4809 vibration excitor) is used as an actuator to transmit sine waves of varying frequencies. The sine waves are generated by NI PCI 6251 and are amplified with a Brüel & Kjær type 2706 power amplifier. A sine-sweep vibration testing approach is adopted where sine waves are swept from 100Hz-20,000Hz. By drilling small holes at both ends of the sample, the vibration excitor nob and two accelerometers (Kistler 8774 A50 with sensitivity 100 mV/g) are mounted.

The input and output acceleration data are acquired by data acquisition module NI USB 9162 and 24 bit NI 9234. The result obtained is postprocessed by a computer system that is connected with data acquisition module and built-in LabView program. The response spectrum is calculated by $T(\mathrm{dB}) = 20\log_{10}(a_{\mathrm{out}}/a_{\mathrm{in}})$ where a_{out}, a_{in} are the output and input acceleration quantities obtained from the output and input accelerometers, respectively.

Method

A monoatomic mass-spring chain is developed to calculate the acoustic mode frequency and compare it with numerically obtained BG opening frequency. Numerical simulation is conducted by two different FEA codes, COMSOL Multiphysics 5.4® and ANSYS R1 2020® to double check the accuracy. The band structures are obtained from COMSOL Multiphysics due to the flexibility in applying Floquet-Bloch periodicity condition. Subsequently a frequency response study is performed by both FEA codes to visualize the vibration attenuation capability for three-dimensional BG frequencies. Both FEA codes yield very agreeable response spectra. The 3D prototypes are developed by using 3D printing technology (OBJECT60 *Strata Sys Ltd*) and vibration test is conducted to validate the numerical findings. Throughout the study, an excellent agreement between theoretical, numerical and experimental results is reported.

Conclusion

This study proposes two optimized phononic metastructures prototypes that govern extremely wide bandgap for vibration and noise filtration and attenuation. The study is conducted by a finite element approach and the numerical solutions are validated by experiments. Initially, an analytical model based on monoatomic mass-spring chain is established to study the bandgap opening and later numerical simulation is performed to obtain the band structure and global and local vibration modes. Both results are in excellent agreement. The band structure of proposed prototypes witnesses the presence of an extremely wide bandgap that is distributed over a wide frequency range. A global mode participation by rigid masses and flexural stiffness of beams results in the opening of bandgap. The bandgap is closed by local mode participation caused by flexural stiffness of the frame assembly while rigid cylindrical masses have no significant contribution. The significant differences between these opening and closing eigenmodes caused by proper engineering design result in ultrawide bandgaps. Further, a supercell structure is created and by conducting a frequency response

study, transmission curves are obtained that confirm the vibration attenuation inside the bandgaps. By additive manufacturing, 3D prototypes are printed and vibration tests are performed to further corroborate our findings. Both numerical simulation and experimental results showed excellent agreement. In the light of this study, the proposed designs can have potential applications in vibration absorption facilities to attenuate noises and vibrations at a wide frequency spectrum. The usage of a single material and simple structural designs make the fabrication and manufacturing works easy. This study may contribute in the design of novel metadevices for elastic and acoustic waves manipulation, and underwater acoustic applications where ultrawide bandgap and wave attenuation is desirable.

References

1 Hussein, M. I., Leamy, M. J. & Ruzzene, M. Dynamics of Phononic Materials and Structures: Historical Origins, Recent Progress, and Future Outlook. *Applied Mechanics Reviews* **66**, 040802, doi:10.1115/1.4026911 (2014).

2 Muhammad & Lim, C. W. From photonic crystals to seismic metamaterials: a review via phononic crystals and acoustic metamaterials. *Applied Mechanics Reviews (under review)* (2020).

3 Muhammad *et al.* Surface elastic waves whispering gallery modes based subwavelength tunable waveguide and cavity modes of the phononic crystals. *Mechanics of Advanced Materials and Structures* **27**, 1053-1064, doi:10.1080/15376494.2020.1728451 (2020).

4 Li, P. & Biwa, S. The SH0 wave manipulation in graded stubbed plates and its application to wave focusing and frequency separation. *Smart Materials and Structures* **28**, 115004, doi:10.1088/1361-665x/ab3ef0 (2019).

5 Liang, Z. & Li, J. Extreme acoustic metamaterial by coiling up space. *Phys Rev Lett* **108**, 114301, doi:10.1103/PhysRevLett.108.114301 (2012).

6 Muhammad & Lim, C. W. Analytical modeling and computation on topological properties of protected interface state of 1-d phononic crystal in elastic media. *Journal of Mechanics of Materials and Structures* **15**, 15-35, doi:DOI: 10.2140/jomms.2020.15.15 (2020).

7 Muhammad, Zhou, W. & Lim, C. W. Topological edge modeling and localization of protected interface modes in 1D phononic crystals for longitudinal and bending elastic waves. *International Journal of Mechanical Sciences* **159**, 359-372, doi:10.1016/j.ijmecsci.2019.05.020 (2019).

8 Zhou, W., Su, Y., Muhammad, Chen, W. & Lim, C. W. Voltage-controlled quantum valley Hall effect in dielectric membrane-type acoustic metamaterials. *International Journal of Mechanical Sciences* **172**, 105368, doi:10.1016/j.ijmecsci.2019.105368 (2020).

9 Allam, A., Sabra, K. & Erturk, A. 3D-Printed Gradient-Index Phononic Crystal Lens for Underwater Acoustic Wave Focusing. *Physical Review Applied* **13**, 064064, doi:10.1103/PhysRevApplied.13.064064 (2020).

10 Cai, Z. *et al.* Bubble Architectures for Locally Resonant Acoustic Metamaterials. *Advanced Functional Materials* **29**, 1906984, doi:10.1002/adfm.201906984 (2019).

11 Huang, Z. *et al.* Bioinspired Patterned Bubbles for Broad and Low-Frequency Acoustic Blocking. *ACS Applied Materials & Interfaces* **12**, 1757-1764, doi:10.1021/acsami.9b15683 (2020).

12 Acar, G. & Yilmaz, C. Experimental and numerical evidence for the existence of wide and deep phononic gaps induced by inertial amplification in two-dimensional solid structures. *Journal of Sound and Vibration* **332**, 6389-6404, doi:10.1016/j.jsv.2013.06.022 (2013).
13 Zhang, Y. Y., Wu, J. H., Hu, G. Z. & Wang, Y. C. Flexural wave suppression by an elastic metamaterial beam with zero bending stiffness. *Journal of Applied Physics* **121**, 134902, doi:10.1063/1.4979686 (2017).
14 Zhou, W. J., Muhammad, Chen, W. Q., Chen, Z. Y. & Lim, C. W. Actively controllable flexural wave band gaps in beam-type acoustic metamaterials with shunted piezoelectric patches. *Eur J Mech a-Solid* **77**, 103807, doi: 10.1016/j.euromechsol.2019.103807 (2019).
15 Muhammad & Lim, C. W. Dissipative multiresonant pillared and trampoline metamaterials with amplified local resonance bandgaps and broadband vibration attenuation. *Journal of Vibration and Acoustics* **142**, 061012, doi:10.1115/1.4047358 (2020).
16 Barnhart, M. V. *et al.* Experimental demonstration of a dissipative multi-resonator metamaterial for broadband elastic wave attenuation. *Journal of Sound and Vibration* **438**, 1-12, doi:10.1016/j.jsv.2018.08.035 (2019).
17 Lu, Y., Yang, Y., Guest, J. K. & Srivastava, A. 3-D phononic crystals with ultra-wide band gaps. *Sci Rep* **7**, 43407, doi:10.1038/srep43407 (2017).
18 D'Alessandro, L., Belloni, E., Ardito, R., Corigliano, A. & Braghin, F. Modeling and experimental verification of an ultra-wide bandgap in 3D phononic crystal. *Applied Physics Letters* **109**, 221907, doi:10.1063/1.4971290 (2016).
19 D'Alessandro, L., Ardito, R., Braghin, F. & Corigliano, A. Low frequency 3D ultra-wide vibration attenuation via elastic metamaterial. *Sci Rep* **9**, 8039, doi:10.1038/s41598-019-44507-6 (2019).
20 D'Alessandro, L., Zega, V., Ardito, R. & Corigliano, A. 3D auxetic single material periodic structure with ultra-wide tunable bandgap. *Sci Rep* **8**, 2262, doi:10.1038/s41598-018-19963-1 (2018).
21 Chen, Y. Y., Hu, G. K. & Huang, G. L. An adaptive metamaterial beam with hybrid shunting circuits for extremely broadband control of flexural waves. *Smart Materials and Structures* **25**, 105036, doi:10.1088/0964-1726/25/10/105036 (2016).
22 Chen, Y., Huang, G. & Sun, C. Band gap control in an active elastic metamaterial with negative capacitance piezoelectric shunting. *Journal of Vibration and Acoustics* **136**, 061008 (2014).
23 Bilal, O. R. & Hussein, M. I. Trampoline metamaterial: Local resonance enhancement by springboards. *Applied Physics Letters* **103**, 111901, doi: 10.1063/1.4820796 (2013).
24 Muhammad, Lim, C. W. & Reddy, J. N. Built-up structural steel sections as seismic metamaterials for surface wave attenuation with low frequency wide bandgap in layered soil medium. *Eng Struct* **188**, 440-451, doi:10.1016/j.engstruct.2019.03.046 (2019).
25 Muhammad, Lim, C. W., Li, J. T. H. & Zhao, Z. Lightweight architected lattice phononic crystals with broadband and multiband vibration mitigation characteristics. *Extreme Mechanics Letters* **41**, 100994, doi:10.1016/j.eml.2020.100994 (2020).
26 Lu, Y., Yang, Y., Guest, J. K. & Srivastava, A. 3-D phononic crystals with ultra-wide band gaps. *Scientific Reports* **7**, 43407, doi:10.1038/srep43407 (2017).
27 D'Alessandro, L., Ardito, R., Braghin, F. & Corigliano, A. Low frequency 3D ultra-wide vibration attenuation via elastic metamaterial. *Scientific Reports* **9**, 8039, doi:10.1038/s41598-019-44507-6 (2019).
28 Chen, Y. & Wang, L. Bio-inspired heterogeneous composites for broadband vibration mitigation. *Scientific Reports* **5**, 17865, doi:10.1038/srep17865 (2015).
29 Muhammad & Lim, C. W. Elastic waves propagation in thin plate metamaterials and evidence of low frequency pseudo and local resonance bandgaps. *Physics Letters A* **383**, 2789-2796, doi:10.1016/j.physleta.2019.05.039 (2019).

30 Delpero, T., Schoenwald, S., Zemp, A. & Bergamini, A. Structural engineering of three-dimensional phononic crystals. *Journal of Sound and Vibration* **363**, 156-165, doi:https://doi.org/10.1016/j.jsv.2015.10.033 (2016).
31 D'Alessandro, L., Belloni, E., Ardito, R., Braghin, F. & Corigliano, A. Mechanical low-frequency filter via modes separation in 3D periodic structures. *Applied Physics Letters* **111**, 231902, doi: 10.1063/1.4995554 (2017).
32 Kennedy, J. *et al.* The Influence of Additive Manufacturing Processes on the Performance of a Periodic Acoustic Metamaterial. *International Journal of Polymer Science* **2019**, 7029143, doi:10.1155/2019/7029143 (2019).
33 Saini, J., Dowling, L., Kennedy, J. & Trimble, D. Investigations of the mechanical properties on different print orientations in SLA 3D printed resin. *Proceedings of the Institution of Mechanical Engineers, Part C: Journal of Mechanical Engineering Science* **234**, 2279-2293, doi:10.1177/0954406220904106 (2020).

Acknowledgment

The work described in this paper was supported by Shenzhen Science and Technology Funding Program (Project No. JCYJ20170413141248626). The authors are also thankful to Jiajia Ren of Department of Architecture and Civil Engineering, City University of Hong Kong for helping in building the geometry and fruitful discussion. The authors are also thankful to Mr. Chi Kin Lai and Mr. Yiu Cheung Wong of Department of Architecture and Civil Engineering, City University of Hong Kong for helping in the printing of 3D prototypes and preparing the experiment setup.

Supplementary materials

The supplementary material is available at (URL).

Declaration of Competing Interest

The authors declare no competing financial interest or personal relationship that could appear to influence the work reported in this paper.

ORCID: The ORCID of Muhammad is 0000-0003-3492-0123; the ORCID of C.W. Lim is 0000-0003-1030-9063

Figures

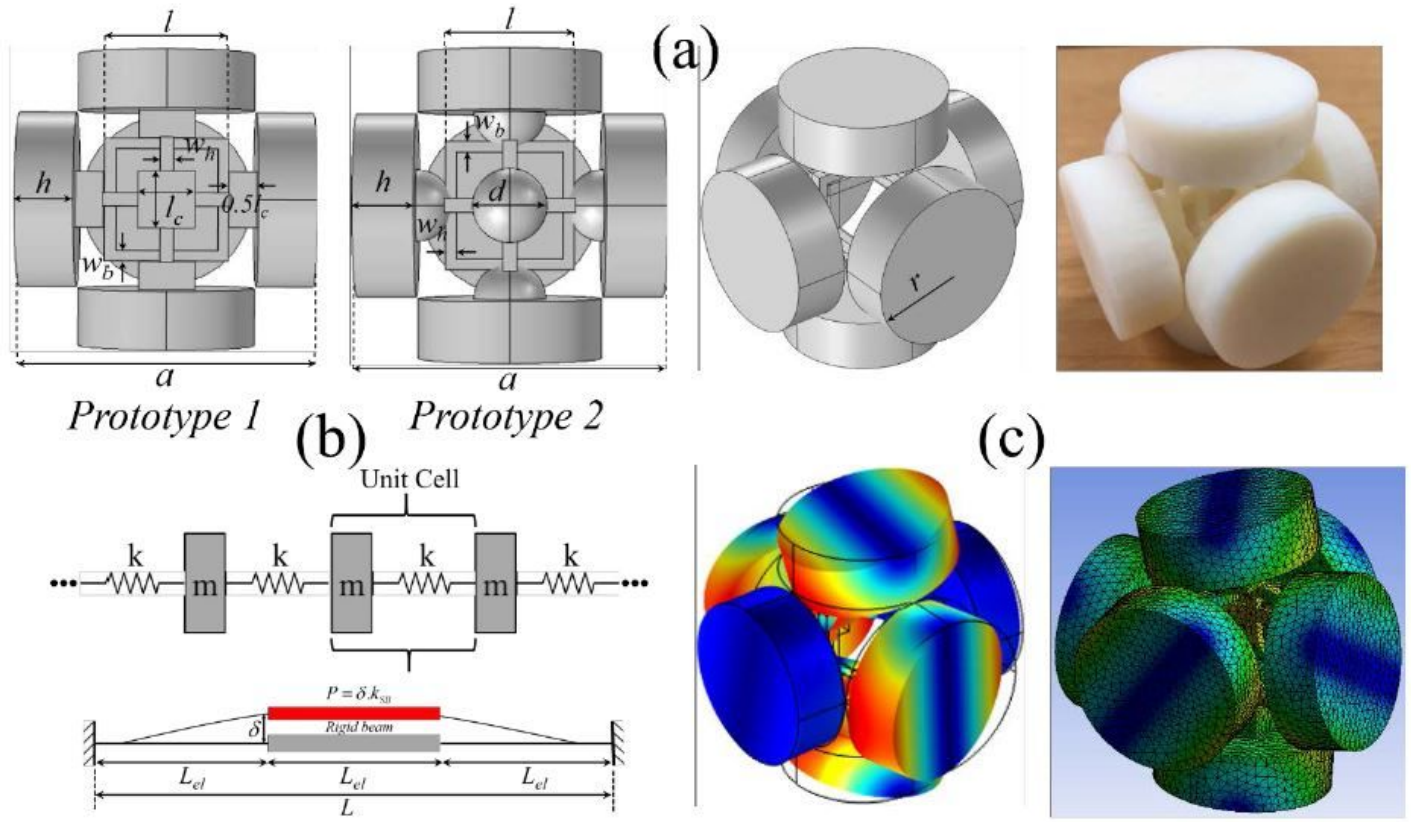

Figure 1

Proposed prototypes for 3D phononic metastructures. (a) Schematic description for prototype 1-2 with 3D printed sample. (b) Monoatomic mass-spring chain along with simplified beam structure. (c) Vibration mode for the lower bounding edge of first BG by COMSOL Multiphysics 5.4® (left) and ANSYS 2020 R1® (right). The analytical and FEA results comparison is presented in Table. 2.

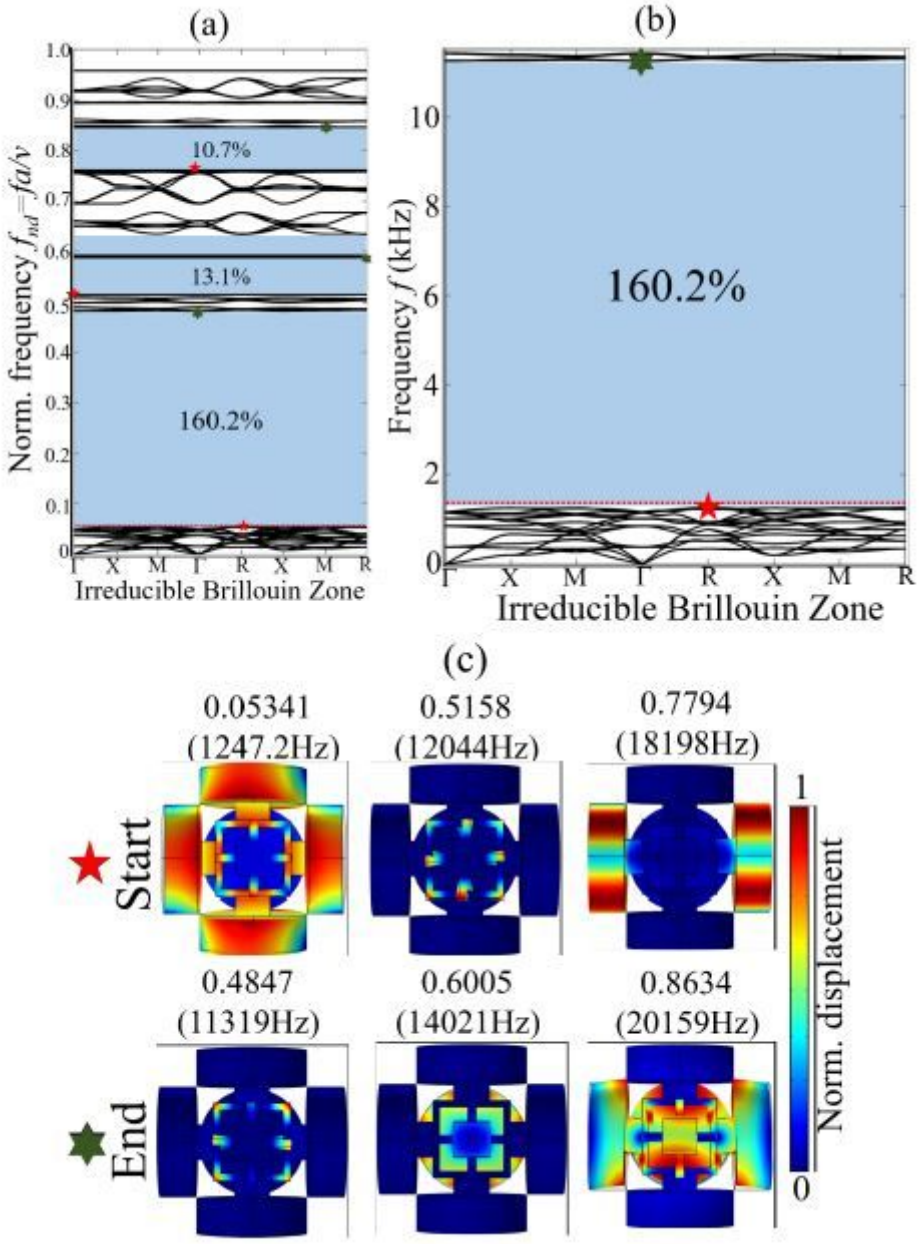

Figure 2

Prototype 1- numerical dispersion spectra: (a) complete band structure with normalized frequency; (b) the widest first BG with Δω/ωc of 160.2%; (c) vibration modes corresponding to the lower and upper bounding edges of BGs.

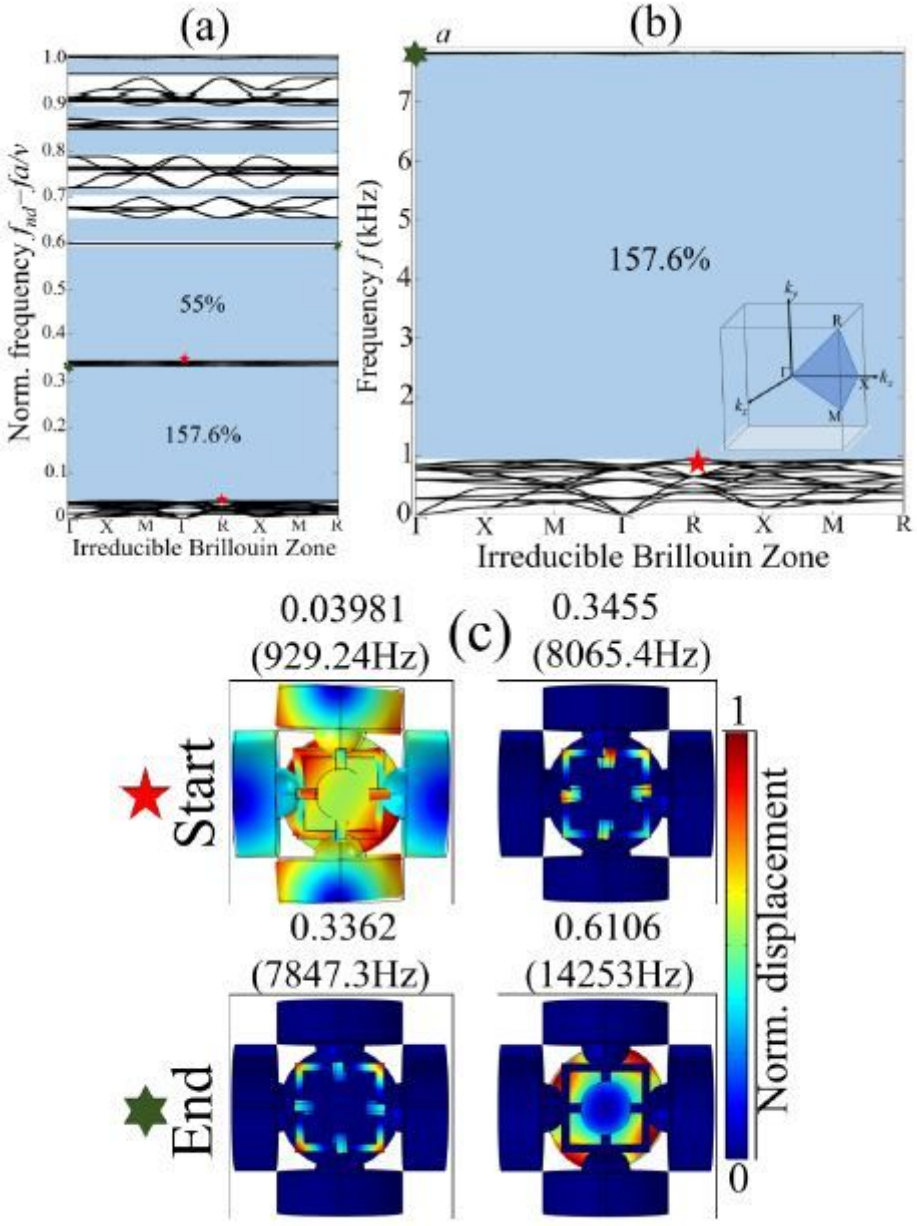

Figure 3

Prototype 2- numerical dispersion spectra: (a) complete band structure with normalized frequency; (b) the widest first BG with Δω/ωc of 157.6%; and (c) vibration modes corresponding to the lower and upper bounding edges of BGs.

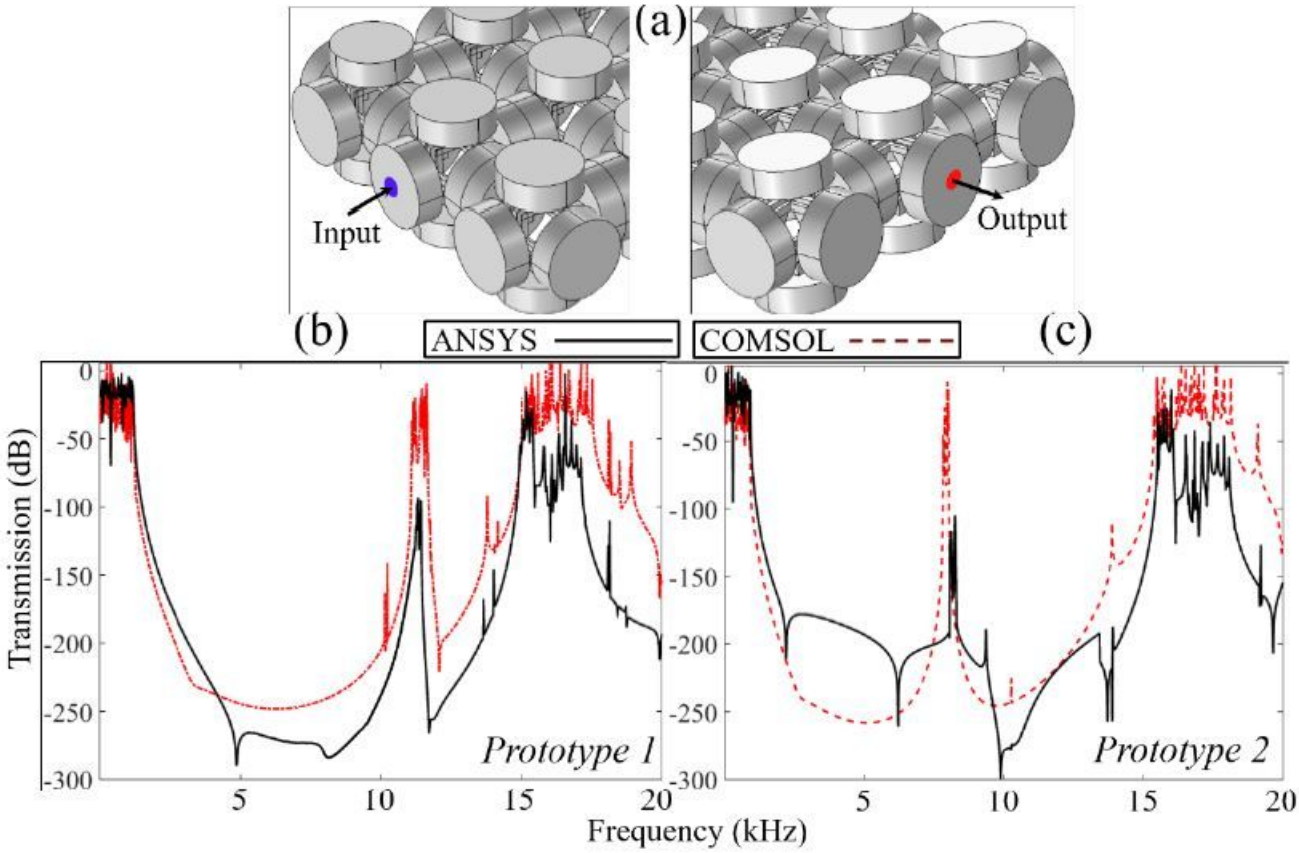

Figure 4

(a) Finite supercell with input (blue) and output (red) probes; (b-c) response spectrum for Prototype 1 and Prototype 2 obtained from COMSOL Multiphysics (red dashed line) and ANSYS workbench (black solid line).

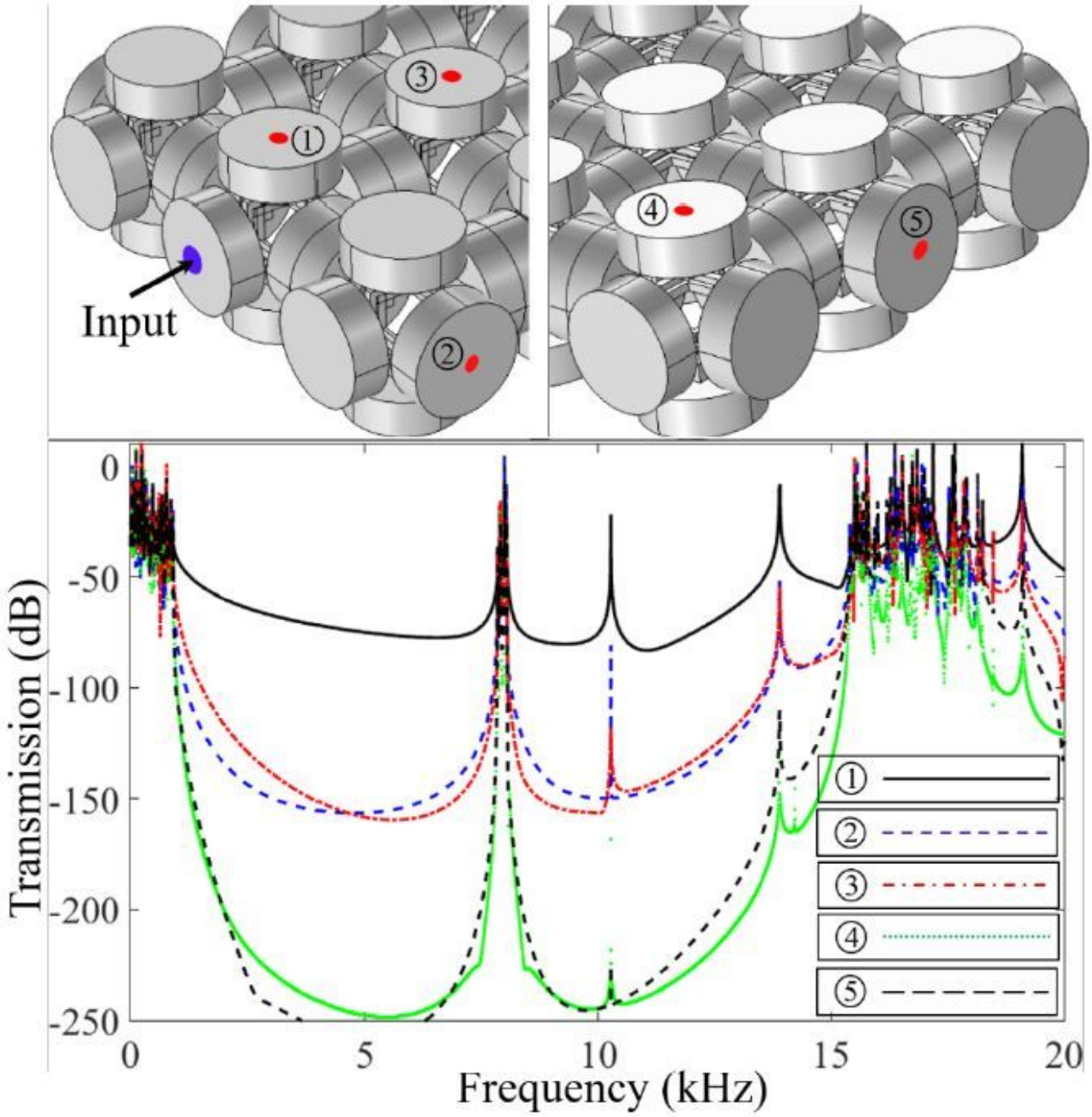

Figure 5

Prototype 2: displacement fields recorded at various probe locations numbered from 1 to 5. The BG width is independent of probe location while the attenuation depth increases if the point probe is away from the excitation source.

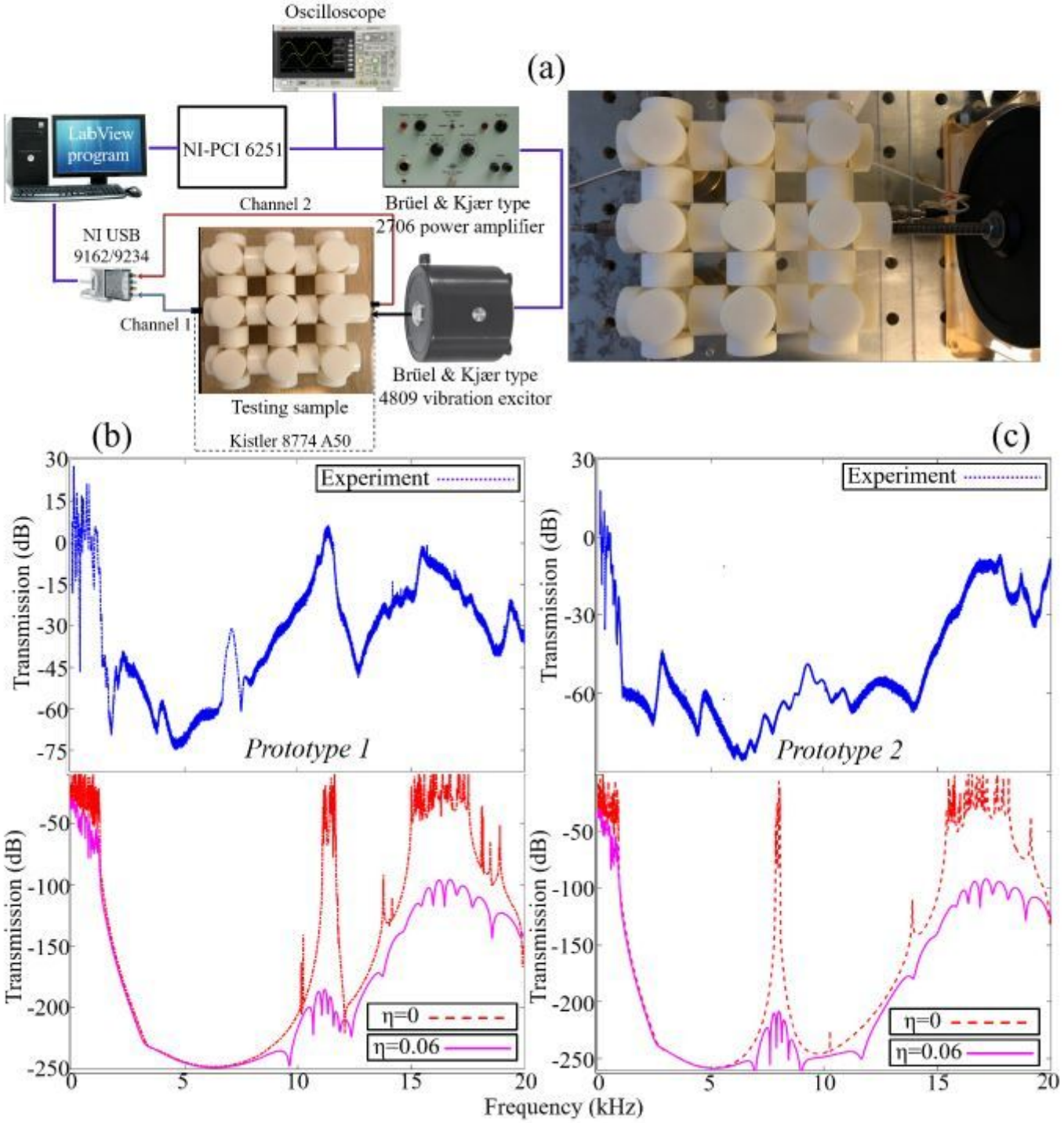

Figure 6

(a) Experiment setup; (b- c) Prototype 1 and Prototype 2 experiment and numerical result. For numerical transmission curve, the effect of material loss factor is η=0.06. Excellent agreement between numerical and experiment result is obtained.

Supplementary Files

This is a list of supplementary files associated with this preprint. Click to download.

- SRSupMate.pdf
- GraphicalAbstract.JPG